
^{99m}Tc -Labeled C2A Domain of Synaptotagmin I as a Target-Specific Molecular Probe for Noninvasive Imaging of Acute Myocardial Infarction

Ming Zhao¹, Xiaoguang Zhu¹, Shundong Ji², Jundong Zhou¹, Kutlan S. Ozker³, Wei Fang⁴, Robert C. Molthen⁵, and Robert S. Hellman³

¹Department of Biophysics, Medical College of Wisconsin, Milwaukee, Wisconsin; ²First Affiliated Hospital of SuZhou University, JiangSu Institute of Hematology, SuZhou, China; ³Department of Radiology, Medical College of Wisconsin, Milwaukee, Wisconsin; ⁴Department of Nuclear Medicine, Fuwai Hospital, Beijing, China; and ⁵Department of Medicine—Pulmonary and Critical Care, Medical College of Wisconsin, Milwaukee, Wisconsin

The exposure of phosphatidylserine (PtdS) is a common molecular marker for both apoptosis and necrosis and enables the simultaneous detection of these distinct modes of cell death. Our aim was to develop a radiotracer based on the PtdS-binding activity of the C2A domain of synaptotagmin I and assess ^{99m}Tc -C2A-GST (GST is glutathione S-transferase) using a reperfused acute myocardial infarction (AMI) rat model. **Methods:** The binding of C2A-GST toward apoptosis and necrosis was validated in vitro. After labeling with ^{99m}Tc via 2-iminothiolane thiolation, radiochemical purity and radiostability were tested. Pharmacokinetics and biodistribution were studied in healthy rats. The uptake of ^{99m}Tc -C2A-GST within the area at risk was quantified by direct γ -counting, whereas nonspecific accumulation was estimated using inactivated ^{99m}Tc -C2A-GST. In vivo planar imaging of AMI in rats was performed on a γ -camera using a parallel-hole collimator. Radioactivity uptake was investigated by region-of-interest analysis, and postmortem tetrazolium staining versus autoradiography. **Results:** Fluorescently labeled and radiolabeled C2A-GST bound both apoptotic and necrotic cells. ^{99m}Tc -C2A-GST had a radiochemical purity of $>98\%$ and remained stable. After intravenous injection, the uptake in the liver and kidneys was significant. For ^{99m}Tc -C2A-GST, radioactivity uptake in the area at risk reached between 2.40 and 2.63 %ID/g (%ID/g is percentage injected dose per gram) within 30 min and remained plateaued for at least 3 h. In comparison, with the inactivated tracer the radioactivity reached 1.06 ± 0.49 %ID/g at 30 min, followed by washout to 0.52 ± 0.23 %ID/g. In 7 of 7 rats, the infarct was clearly identifiable as focal uptake in planar images. At 3 h after injection, the infarct-to-lung ratios were 2.48 ± 0.27 , 1.29 ± 0.09 , and 1.46 ± 0.04 for acute-infarct rats with ^{99m}Tc -C2A-GST, sham-operated rats with ^{99m}Tc -C2A-GST, and acute-infarct rats with ^{99m}Tc -C2A-GST-NHS (NHS is *N*-hydroxy succinimide), respectively. The distribution of radioactivity was confirmed by autoradiography

and histology. **Conclusion:** The C2A domain of synaptotagmin I labeled with fluorochromes or a radioisotope binds to both apoptotic and necrotic cells. Ex vivo and in vivo data indicate that, because of elevated vascular permeability, both specific binding and passive leakage contribute to the accumulation of the radiotracer in the area at risk. However, the latter component alone is insufficient to achieve detectable target-to-background ratios with in vivo planar imaging.

Key Words: C2A domain; synaptotagmin I; apoptosis; necrosis; myocardial infarction

J Nucl Med 2006; 47:1367–1374

Noninvasive imaging of cell death has important diagnostic and prognostic predictive potentials. Collectively, the underlying pathologic cause of many degenerative diseases can be attributed to the interplay of different modes of cell death. Among the 2 dominant forms of cell death, apoptosis has gained much attention in modern medicine not only because of the deleterious consequences of its deregulation but also as an opportunity for therapeutic intervention (1–5). The active process of apoptosis is an intracellular, energy-dependent event (6,7). Once committed, the execution phase of apoptosis involves a proteolytic cascade catalyzed by caspases and is accompanied by distinct molecular markers (8–11). In contrast, necrosis is a form of passive cell death recognized by swelling and plasma membrane damage. The characterization of apoptosis and necrosis is likely to dictate the development and implementation of novel imaging technologies.

Acute myocardial infarction (AMI) involves both forms of cell death, although the exact extent of each remains controversial because of variations in animal models and detection methods (12). It has been generally accepted that necrosis occurs at the central ischemic zone, whereas

Received Feb. 26, 2006; revision accepted Apr. 6, 2006.
For correspondence or reprints contact: Ming Zhao, PhD, Department of Biophysics, Medical College of Wisconsin, 8701 Watertown Plank Rd., Milwaukee, WI, 53226.
E-mail: mzhao@mcw.edu
COPYRIGHT © 2006 by the Society of Nuclear Medicine, Inc.

apoptosis is more prevalent in the periphery within the area at risk. In addition, apoptotic cell death involves not only cardiomyocytes but also nonmyocytes to a comparable degree, including vascular endothelium, macrophages, and blood cells (13). Although conventionally AMI has been regarded as a primarily necrotic condition, infarct imaging using necrosis-avid agents has achieved a certain degree of success by targeting necrotic markers, such as calcium deposit, histone, and myosin epitopes (14). The better understanding of different forms of cell death has presented the opportunity to detect multiple, if not all, forms of cell death as a single comprehensive category and, thus, has provided the potential advantage of being more likely to reflect the true extent of irreversible myocardial damage.

A common molecular marker for both apoptosis and necrosis is the exposure of phosphatidylserine (PtdS), and its presence can facilitate target-specific imaging of cell death. In viable cells, PtdS is strictly a constituent of the inner leaflet of the plasma membrane. The asymmetry of the lipid bilayer is maintained by the actions of energy-dependent enzymes, including aminophospholipid translocase and floppase (15). During apoptosis, the inhibition of translocase and floppase is accompanied by the activation of scramblase, and the redistribution of phospholipids across the bilayers is facilitated (15). As a result, PtdS becomes exposed onto the cell surface. In necrotic cells, the passive rupture of the plasma membrane renders intracellular components, including PtdS, accessible to extracellular milieu. As one of the major phospholipid components of the plasma membrane, PtdS provides an abundant molecular marker for the detection of both apoptosis and necrosis once it becomes accessible.

The C2A domain of synaptotagmin I binds to negatively charged phospholipids in membranes, including PtdS, in a calcium-dependent manner (16). C2A labeled with fluorochromes and contrast agents has allowed detection of cell death using fluorescent and MRI techniques, respectively (17,18). The imaging applications of another protein that binds PtdS, annexin V, have also been well documented in a wide range of animal models and clinical studies (19–22). Meanwhile, derivatives of annexin V continue to evolve in the search for improved binding and pharmacokinetic profiles (23,24).

The aim of this study was 2-fold: development of a technetium-based PtdS-binding molecular probe for detecting apoptosis and necrosis and characterization of the imaging tracer within the context of AMI. To date, the uptake of radiolabeled annexin V in acute and chronic infarct has been described in animal models and in human patients (25,26), but key questions remain unresolved. AMI is characterized by a multiplicity of cellular and physiologic changes, not only including various forms of cell death but also markedly elevated vascular permeability and increased interstitial space (27). In fact, these structural changes have become the foundation for delineating infarct areas with MRI using apparently nonspecific contrast

agents (27,28). Therefore, the presence of PtdS-binding radiotracers in the infarct region does not necessarily warrant PtdS interaction but also can be associated with nonspecific leakage of the tracer across the vascular boundary and diffusion into the interstitial space. Here, our investigation was designed to characterize one such radiotracer, ^{99m}Tc -labeled C2A, for its distribution within the area at risk. The C2A was overexpressed and labeled in the form of C2A-GST (GST is glutathione *S*-transferase) fusion protein. The inclusion of GST only moderately increases molecular weight but greatly reduces the probability of chemical modification in the vicinity of the PtdS-binding site on C2A. We show that (a) fluorescently labeled C2A-GST specifically binds to both apoptotic and necrotic cells *in vitro*, (b) the fusion protein can be stably labeled with ^{99m}Tc at a reasonably high radiochemical yield and purity through thiolation using 2-iminothiolane, (c) a high accumulation of ^{99m}Tc -C2A-GST in the area at risk is attributed to both specific binding and passive distribution, and (d) ^{99m}Tc -C2A-GST uptake allows noninvasive visualization of AMI in a rat model using single-photon planar imaging, whereas passive leakage alone was insufficient for such detection.

MATERIALS AND METHODS

C2A-GST was overexpressed in *Escherichia coli* and purified as described previously (16). The protein was dialyzed in phosphate-buffered saline (PBS) (pH 7.4), lyophilized, and stored at -20°C .

Fluorescein Isothiocyanate (FITC) Labeling of C2A-GST and Cell Assays

Three hundred microliters of C2A-GST (2 mg/mL) in PBS were mixed with 2.33 μL of FITC (12 mg/mL in dimethyl sulfoxide [DMSO]) and gently shaken for 3 h at room temperature. C2A-GST-FITC was purified using a Sephadex G-25 column equilibrated with PBS.

Apoptosis was induced in Jurkat cells (American Type Culture Collection) at a density of 5×10^6 cells/mL with 3.5 $\mu\text{mol/L}$ camptothecin (Sigma) for 3 h. C2A-GST-FITC and propidium iodide (PI) were added to final concentrations of 1 and 5 $\mu\text{g/mL}$, respectively. The sample was analyzed by 2-color flow cytometry. In parallel, the same cells were analyzed with commercial annexin V-FITC (Sigma; 1 $\mu\text{g/mL}$) and PI (5 $\mu\text{g/mL}$) according to the manufacturer's instructions.

To test whether both C2A-GST and annexin V recognize the same apoptotic or necrotic cells, C2A-GST was labeled with Alexa Fluor 680 (AF680; Molecular Probes). Specifically, 250 μL of C2A-GST (2 mg/mL; 100 mmol/L NaHCO_3 , 60 mmol/L NaCl , pH 8.2) were mixed with 12.4 μL of AF680 (1 mg/mL in methanol). After 1 h at room temperature while shielded from light, the conjugate was purified using G-25 Sephadex chromatography. C2A-GST-AF680 was incubated, in the direct presence of annexin V-FITC, with treated Jurkat cells and analyzed with flow cytometry to detect C2A-GST-positive cells (red) and annexin V-positive cells (green).

^{99m}Tc Labeling of C2A-GST

C2A-GST was labeled with ^{99m}Tc in a 2-step process (29). Specifically, 200 μL of C2A-GST (2 mg/mL) solution in PBS

were mixed with 2.96 μL of 2-iminothiolane (10 mg/mL in DMSO) and incubated at 37°C for 1 h. Then 500 μL of $^{99\text{m}}\text{TcO}_4^-$ in 0.9% NaCl were added to a stannous glucoheptonate mixture (80 μg stannous chloride and 8 mg sodium glucoheptonate) and incubated at room temperature for 10 min under N_2 . Four hundred microliters of $^{99\text{m}}\text{Tc}$ -glucoheptonate were mixed with 200 μL of thiolated C2A-GST and incubated for 30 min at room temperature. $^{99\text{m}}\text{Tc}$ -C2A-GST was purified using Sephadex G-25 chromatography.

The radiochemical purity (RCP) of $^{99\text{m}}\text{Tc}$ -C2A-GST and the presence of $^{99\text{m}}\text{Tc}$ -colloid were analyzed by instant thin-layer chromatography (ITLC-SG; Gelman Sciences) using 2 solvent systems as the mobile phase: saline and $\text{NH}_3\cdot\text{H}_2\text{O}/\text{alcohol}/\text{H}_2\text{O}$ (1:2:5, v/v/v).

The stability of $^{99\text{m}}\text{Tc}$ -C2A-GST was assessed by incubating $^{99\text{m}}\text{Tc}$ -C2A-GST (10 μL , 0.2 mg/mL) in 500 μL saline, rat serum, or whole blood at room temperature. The RCP was measured by ITLC at 1, 2, 4, and 24 h with corrections for decay. The degree of thiolation was estimated using Ellman's reagent (30). For control purposes, inactive $^{99\text{m}}\text{Tc}$ -C2A-GST was produced by reacting with 2 mmol/L sulfo-*N*-hydroxy succinimide (NHS) acetate for 15 min at room temperature and purified.

In Vitro Binding Assays

About 1 μg of $^{99\text{m}}\text{Tc}$ -C2A-GST was incubated with 500 μL of apoptotic or untreated cells (5×10^5) in 15 mmol/L *N*-(2-hydroxyethyl) piperazine-*N'*-(2-ethanesulfonic acid) (HEPES), 120 mmol/L NaCl, 2 mmol/L CaCl_2 , pH 7.4. A parallel sample was prepared using $^{99\text{m}}\text{Tc}$ -C2A-GST-NHS as the control. To separate cell-bound from free $^{99\text{m}}\text{Tc}$ -C2A-GST, the mixture was centrifuged at 1,000g for 2 min through 100 μL of silicon oil. After removing the aqueous supernatant and oil layer, the tip of each tube that contained the pellet was cut off and its radioactivity was measured by γ -counting.

Binding specificity after radiolabeling was evaluated using a competition assay. Specifically, $^{99\text{m}}\text{Tc}$ -C2A-GST (78 nmol/L) was incubated with 5×10^5 camptothecin-treated Jurkat cells in the presence of unlabeled C2A-GST from 15.9 to 7,830 nmol/L. The radioactivity that remained bound to the cells was calculated as a percentage of that without competition and plotted against the concentration of unlabeled C2A-GST. The 50% inhibitory concentration (IC_{50}) at this particular experimental condition was the concentration of unlabeled C2A-GST required to reduce the binding of $^{99\text{m}}\text{Tc}$ -C2A-GST by 50% (B_{50}).

Blood Half-Life and Biodistribution Studies in Normal Rats

Animal procedures were conducted following National Institutes of Health guidelines and with institutional approval. Blood clearance of $^{99\text{m}}\text{Tc}$ -C2A-GST or $^{99\text{m}}\text{Tc}$ -C2A-GST-NHS was studied in anesthetized healthy male Sprague-Dawley rats (8- to 10-wk old; $n = 5$). $^{99\text{m}}\text{Tc}$ -C2A-GST (46 μg) was injected via a left femoral vein catheter. Ten microliters of blood were sampled from a right femoral artery catheter at 0.5, 5, 10, 15, 20, 30, 40, 60, 120, and 180 min after injection. The blood radioactivity was measured by γ -counting.

For biodistribution, each rat was injected with 3.7 MBq of $^{99\text{m}}\text{Tc}$ -C2A-GST via the femoral vein. One group of 5 rats was sacrificed at 10, 30, 60, and 180 min after injection. The radioactivity uptake was measured for blood, heart, lung, spleen, liver, kidney, stomach, small intestine, large intestine, bone, muscle, fat,

and skin by γ -counting using an energy window between 120 and 160 keV. Data are expressed in terms of percentage injected dose per gram or per organ \pm SD (%ID/g \pm SD or %ID/organ \pm SD). Blood, muscle, and bone were assumed to represent 7%, 40%, and 10% of body weight, respectively. The percentages of fat and skin of whole-body weight are unavailable and, thus, are not included as %ID/organ.

Uptake Study in Rat Model of AMI

This procedure is to quantify the absolute tracer uptake in the area at risk versus viable myocardium at different times after injection. Here, we used an acute infarct model with 18 min of ischemia followed by 2 h of reperfusion. With this model we have confirmed the presence of acute infarction using triphenyl tetrazolium chloride (TTC) staining. Acute infarct models using a short duration of ischemia have also been reported elsewhere (28,31).

For each anesthetized rat, after tracheotomy and intubation, respiration was maintained using a rodent respirator. After thoracotomy, the left descending coronary artery was ligated for 18 min using a 6.0 suture at 1 mm below the left atrial appendage. After reperfusion, the loose suture was left in place until sacrifice, when an area-at-risk measurement was made. $^{99\text{m}}\text{Tc}$ -C2A-GST (\sim 7.4 MBq) was injected via the femoral vein at 2 h of reperfusion. A group of 4 rats was sacrificed at 10, 30, 60, and 180 min after injection. The left descending coronary artery was reoccluded at 30 s before sacrifice and 2 mL of Evans Blue (2% in PBS, w/v) were injected into the femoral vein to stain perfused myocardium. The myocardium devoid of Evans Blue was considered as the area at risk. After dissecting and weighing the heart tissues, tracer uptake in the area at risk and normal myocardium was determined separately by γ -counting. The results are expressed as %ID/g \pm SD. To quantify nonspecific uptake, $^{99\text{m}}\text{Tc}$ -C2A-GST-NHS was studied using an identical protocol.

To investigate whether the uptake of $^{99\text{m}}\text{Tc}$ -C2A-GST is associated with the treatment of ischemia or reperfusion per se, the above experiment was repeated with 5 min of ischemia followed by 2 h of reperfusion.

Histology

Terminal deoxynucleotidyl transferase-mediated dUTP nick-end labeling (TUNEL) was performed according to the manufacturer's protocol, using 10- μm short-axis cryosections of the heart. At least 3,500 nuclei were counted from random fields within the area at risk or in the normal region, under a magnification of \times 400. The apoptotic index was calculated in terms of TUNEL-positive nuclei as a percentage of total nuclei. For electron microscopy (EM), specimens from the area at risk and the normal myocardium were fixed in 4% paraformaldehyde and 0.5% glutaraldehyde for 24 h at 4°C. The tissues were dehydrated, sectioned, and mounted on carbon grids for transmission EM.

In Vivo Imaging of AMI in Rat Model

Reperfused ischemic injury was created in rats as described. To examine the background tracer uptake, we included sham-operated rats with identical surgery except for coronary occlusion. Either $^{99\text{m}}\text{Tc}$ -C2A-GST or $^{99\text{m}}\text{Tc}$ -C2A-GST-NHS was injected via the femoral vein at a dosage of \sim 37 MBq, and anterior planar images of each rat in prone position were acquired using an Infinia (GE Healthcare) γ -camera and parallel-hole collimator with a 15% energy window centering at 140 keV. A reference radiation source was positioned on the left side of the animal. The field of

view was 22.5×22.5 mm with a 512×512 matrix. Each image was acquired with 1 million counts at 0, 40, 80, 120, 160, and 200 min after injection. Heart-to-lung ratios were estimated using region-of-interest analysis.

Autoradiography

After the rat was sacrificed, the heart was harvested and quickly rinsed in saline. About 2 mL of 0.5% TTC in HEPES buffer (w/v) was infused retrograde into the aorta to stain the entire myocardium. After 15 min of incubation at 37°C , the heart was fixed in 4% formaldehyde. Short-axis sections of the heart with a thickness of ~ 500 μm were cut and exposed to Kodak BMX MS film overnight at -80°C . After the film was developed, each corresponding slice was fixed overnight in 1% formaldehyde in PBS (v/v). Digitized autoradiography and histology section images were inspected visually.

RESULTS

The fusion protein has a molecular weight of 39,687 Da, with 346 amino acids, of which 130 are from C2A and 201 are from GST. The flexible linker sequence contains 15 residues, in which a thrombin cleavage site is included. There are 14 Lys and no Cys in C2A and 19 Lys and 4 Cys in GST, with the flexible linker peptide containing neither residue.

FITC Labeling of C2A-GST and In Vitro Studies

The fluorescein-to-protein ratio of C2A-GST-FITC was estimated to be 1.1 ± 0.2 . To test the binding activity for apoptotic and necrotic cells, C2A-GST-FITC was incubated with control or camptothecin-treated Jurkat cells and analyzed using flow cytometry. As shown in Figures 1A and 1B, distinct cell populations were detected as viable (V), apoptotic (A), and necrotic (N). In addition, a presumably early apoptotic (EA) population was identified with intermediate fluorescent intensity. These cells appear to be at a transitional state toward fully developed apoptosis or necrosis; yet they are negative for PI. A nearly identical flow cytometric profile was obtained in a parallel staining study using a commercial annexin V staining kit, which is regarded as a gold standard for in vitro cell viability analysis (Figs. 1C and 1D).

To further evaluate the binding specificity of C2A-GST, double staining of camptothecin-treated Jurkat cells was performed with coinubation of C2A-GST-AF680 (red) and annexin V-FITC (green) and analyzed by dual-color flow cytometry. Simultaneous uptake of both red and green fluorescence was seen in each positive cell (Fig. 1E), whereas the viable cells were negative. There was clearly an absence of single positive cells for either color. The 2 fluorochromes were selected to minimize emission spectra overlap, where the emission wavelength of AF680 is near-infrared and FITC is in the green fluorescence range (Fig. 1E).

$^{99\text{m}}\text{Tc}$ Labeling of C2A-GST

According to Ellman's method, each molecule of C2A-GST contains an average of 2.87 and 7.15 thiols before and after iminothiolation, respectively. The radiochemical yield

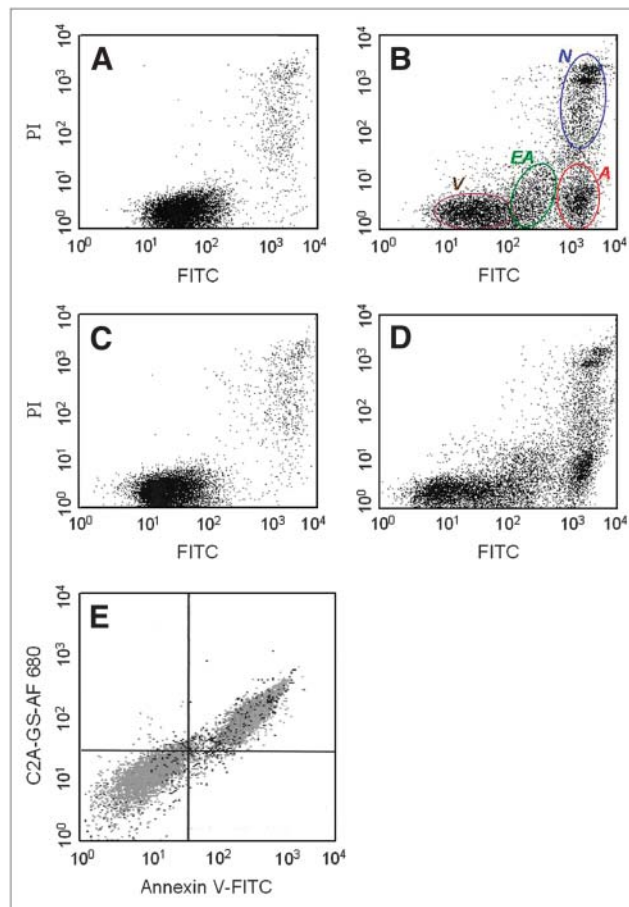


FIGURE 1. Flow cytometry of control (A and C) and camptothecin-treated (B and D) Jurkat cells, with FITC-labeled C2A-GST (A and B) and annexin V (C and D) and costaining with PI and double staining using C2A-GST-AF680 and annexin V-FITC (E). Four distinct populations identified by C2A-GST-FITC are illustrated in B, including viable (V), early apoptotic (EA), apoptotic (A), and necrotic cells (N).

and purity data of the nonthiolated and thiolated C2A-GST are as follows: Before gel-filtration purification, the RCP values for the native and thiolated protein are 12.5% and 72.8%, respectively. After gel-filtration purification, the values are 88.4% and 98.9%, respectively. Under identical labeling conditions, the radiochemical yield is enhanced ~ 4 -fold with thiolation. The stability of the labeled protein was tested in saline, rat whole blood, and rat serum. The protein retained the radiolabel over a 24-h period as determined by ITLC (Table 1).

In Vitro Binding Assays

The uptake and binding specificity of $^{99\text{m}}\text{Tc}$ -C2A-GST were evaluated using camptothecin-treated Jurkat cells as the binding target. For 5×10^5 cells after 3 h of stimulation and incubation with $^{99\text{m}}\text{Tc}$ -C2A-GST, the radioactivity uptake was $9.12\text{-fold} \pm 0.6$ higher than that of the non-treated viable control population. In comparison, $^{99\text{m}}\text{Tc}$ -C2A-GST-NHS showed a 1.88 ± 0.04 times difference

TABLE 1
Stability Test for ^{99m}Tc -C2A-GST

Fluid	0 h	1 h	2 h	4 h	24 h
Saline	99.53	99.53	99.12	98.70	98.42
Rat serum	99.53	96.42	95.70	93.40	91.32
Rat whole blood	99.53	90.85	90.77	90.08	89.17

^{99m}Tc -C2A-GST was incubated with saline, rat serum, or whole blood for 1, 2, 4, and 24 h. RCP was determined using ITLC.

under identical experimental conditions. In the presence of increasing concentrations of unlabeled C2A-GST, the uptake of radioactivity in treated Jurkat cells was competitively inhibited, with a well-defined sigmoid pattern. Using 5×10^5 treated cells and 80 nmol/L ^{99m}Tc -C2A-GST, the IC_{50} of unlabeled C2A-GST was 90.01 ± 11.12 nmol/L ($n = 3$). However, the competition profile was absent when unlabeled C2A-GST was replaced with bovine serum albumin, GST, or C2A-GST-NHS.

Biodistribution and Blood Clearance

The distribution of radioactivity after intravenous injection of ^{99m}Tc -C2A-GST in healthy rats is summarized as a function of time (Fig. 2). The most prominent organs of uptake include the liver and kidneys, suggesting hepatic and renal clearance. The presence of radioactivity in the spleen, bones, and lungs was significant, with the latter reflecting the blood-pool activity. In contrast, there is relatively low uptake in viable myocardium, gastrointestinal

tract, adipose tissues, skeletal muscles, and skin. There is no indication that the radiotracer crosses the blood-brain barrier. A low thyroid uptake suggests that there was minimal dissociation of the radioisotope from the labeled protein. The blood clearance of ^{99m}Tc -C2A-GST was typical for a macromolecule of comparable size, with an estimated half-life of the fast clearance phase at <15 min ($n = 5$). No toxicity effect was observed at the current dosage.

Uptake Study in Rat Model of AMI

The uptake of radioactivity in the area at risk versus normal myocardium after ^{99m}Tc -C2A-GST or ^{99m}Tc -C2A-GST-NHS injection in rats was quantified as a function of time using direct γ -counting. As summarized in Figure 3, the radioactivity level in the area at risk after ^{99m}Tc -C2A-GST injection reached 1.91 ± 0.59 %ID/g within the first 10 min after injection and plateaued between 2.40 and 2.63 %ID/g after 30 min. The uptake in normal myocardium was 0.21 ± 0.01 %ID/g at 10 min, with a gradual washout to 0.09 ± 0.04 %ID/g at 180 min. In comparison, radioactivity uptake from ^{99m}Tc -C2A-GST-NHS reached as high as 1.06 ± 0.49 %ID/g at 30 min, presumably due to nonspecific vascular leakage, followed by washout to 0.52 ± 0.23 %ID/g at 180 min. The distribution of ^{99m}Tc -C2A-GST-NHS in normal myocardium over time was similar to that of ^{99m}Tc -C2A-GST. According to above %ID/g measurements, the target-to-background ratio between the area at risk and normal myocardium is 30.4 for ^{99m}Tc -C2A-GST, whereas the ratio is 6.5 for ^{99m}Tc -C2A-GST-NHS at 180 min after injection. TTC staining demonstrates the presence of infarct tissues within the area at risk, indicating

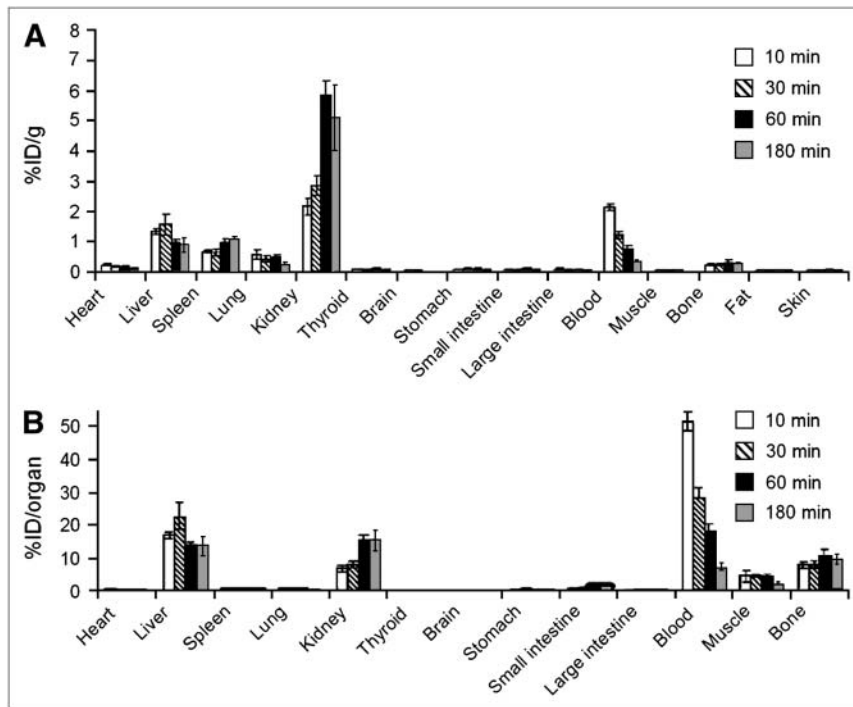


FIGURE 2. Biodistribution of ^{99m}Tc -C2A-GST in healthy rats at 10, 30, 60, and 180 min after injection ($n = 5$). Radioactivity uptake is shown in terms of %ID/g (A) and %ID/organ (B).

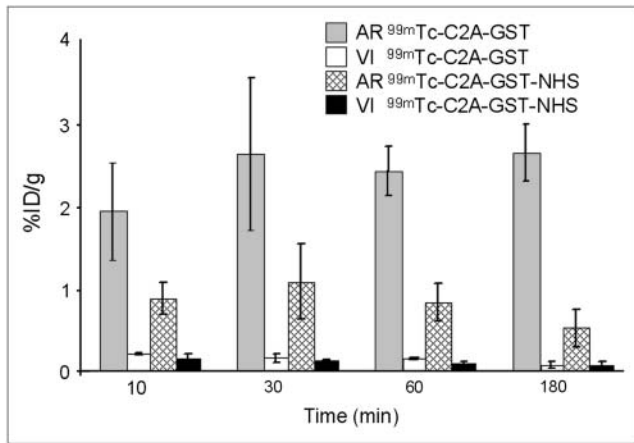


FIGURE 3. Radioactivity uptake, in terms of %ID/g, in rats in area at risk (AR) and in normal (VI) myocardium at 10, 30, 60, and 180 min after intravenous injection of ^{99m}Tc -C2A-GST and ^{99m}Tc -C2A-GST-NHS ($n = 4$).

the occurrence of extensive necrosis. This transition was in parallel with the elevation of apoptotic index from 0.27% to 4.70%. Short stimulation with 5 min of ischemia followed by reperfusion caused no significant uptake of ^{99m}Tc -C2A-GST in the area at risk compared with viable myocardium at 1 h after injection.

In Vivo Imaging of AMI in Rat Model

The biodistribution and uptake data were confirmed by in vivo planar imaging. Prominent hepatic uptake was seen in all cases immediately after radiotracer injection, followed by an increase in signal in the kidneys and bladder over time. As shown in Figure 4A, with the clearance of blood-pool and lung activities, a hot-spot uptake was visible as early as 40 min after injection, consistent with the location of the left anterior region of the left ventricle in infarct animals injected with ^{99m}Tc -C2A-GST. In 7 of 7 rats with an acute infarct, the signal became more focal and distinct over time. In contrast, neither infarct animals injected with ^{99m}Tc -C2A-GST-NHS nor sham-operated rats injected with ^{99m}Tc -C2A-GST showed significant tracer uptake in the left ventricle region (Fig. 4A). At 3 h after injection, the infarct-to-lung ratios were 2.48 ± 0.27 , 1.29 ± 0.09 , and 1.46 ± 0.04 for acute infarct rats injected with ^{99m}Tc -C2A-GST ($n = 7$), sham-operated rats injected with ^{99m}Tc -C2A-GST ($n = 3$), and acute infarct rats injected with ^{99m}Tc -C2A-GST-NHS ($n = 3$), respectively. The presence of radioactivity in the area-at-risk region in rats injected with ^{99m}Tc -C2A-GST was also confirmed by autoradiography and TTC staining (Fig. 4B).

DISCUSSION

This study evaluated a molecular probe, ^{99m}Tc -C2A-GST, and addressed the dynamic uptake profile using quantitative and semiquantitative methods in a rat model

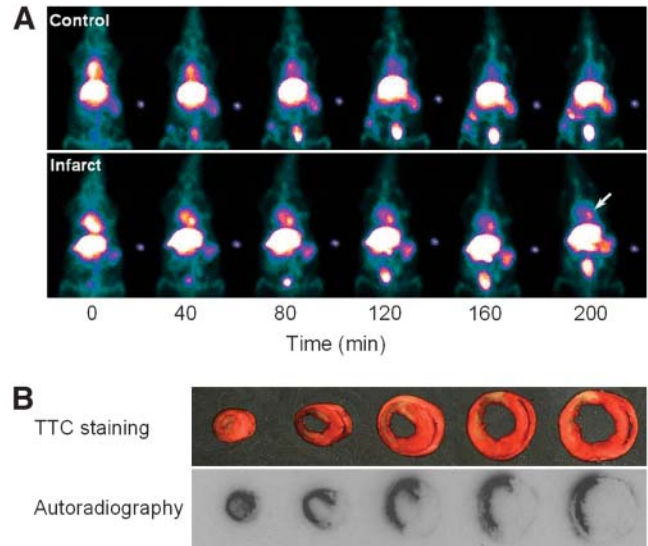


FIGURE 4. (A) In vivo single-photon planar imaging of sham-operated rat (Control) and rat with infarct at 0, 40, 80, 120, 160, and 200 min after intravenous injection of ^{99m}Tc -C2A-GST. Arrow indicates site of the infarct. (B) Corresponding TTC staining and autoradiography images.

of reperfused AMI. The radiotracer targets PtdS as a common marker for both apoptosis and necrosis and detects cell death as a single comprehensive category.

C2A-GST could be readily labeled with fluorochromes or a radioisotope. When fluorescently labeled, apoptosis and necrosis binding activity of the conjugates was comparable to that of annexin V. When coincubated with chemically treated cells in vitro, the 2 PtdS-binding proteins associate with apoptotic and necrotic cells, suggesting that the 2 molecular probes interact with a shared molecular marker, presumably PtdS. C2A and annexin V are 2 structurally distinct proteins, whereas their binding activity is somewhat similar in that they interact with anionic phospholipids in a calcium-dependent fashion (16,31–35). In contrast to annexin family members that assume predominantly helical structures, C2A is a compact β -sandwich (31–35). Given the importance of developing target-specific molecular probes for apoptosis and necrosis, a greater structural diversity should lead to a better chance of discovering isoforms or derivatives that generate favorable binding and pharmacokinetic properties. Although a direct and quantitative comparison between the 2 PtdS-binding proteins is beyond the scope of this study, it warrants further investigation in terms of binding activities, structural properties, and potentials for in vivo applications.

For radiolabeling using ^{99m}Tc , thiolation of the fusion protein was essential, although there are native cysteine residues in native C2A-GST. According to Ellman's method, the native protein contains an average of 2.87 thiols per molecule, whereas the conjugate has an average of 7.15. These data indicate that the conjugation introduced an average of 4.3 thiols per molecule. Although, according to

sequencing there are 4 Cys residues in native C2A-GST, there appears to be a discrepancy between the measured and the actual number of thiol groups in the native protein (2.87 by Ellman's test vs. 4 from sequencing). This could be explained by the 3-dimensional structure of GST (EC 2.5.1.18; *Schistosoma japonicum*), where the side chain of Cys-169 is facing away from the protein surface while the thiol groups of Cys-85, Cys-138, and Cys-178 appear to be exposed and easily accessible. Thus, the outcome of Ellman's test could have reflected the orientation and accessibility of thiol groups to the colorimetric reagent, 5,5'-dithio-bis-(2-nitrobenzoic acid), dissolved in the aqueous environment. The lack of efficient ^{99m}Tc incorporation before iminothiolation suggests that the endogenous thiols do not form favorable chelating sites for the radioisotope. The radiolabeled C2A-GST has a relatively high RCP and good radio-stability. After radiolabeling, ^{99m}Tc -C2A-GST appeared to have retained its binding activity. In vitro, significantly elevated uptake of the radiotracer was detected in camptothecin-treated Jurkat cells compared with that of the control. In addition, the fact that the binding of ^{99m}Tc -C2A-GST was reversible in the presence of competing unlabeled C2A-GST indicates that both forms of C2A-GST specifically interact with the same well-defined binding targets in treated cells and that the binding specificity of ^{99m}Tc -C2A-GST was well preserved.

Successful development of an infarct-avid imaging agent not only relies on an understanding of cell death processes but also is critically dependent on characterization of specific as well as passive distribution of such tracers. Vascular hyperpermeability associated with ischemic challenge have been well documented. This brings up the issue of diffusive leakage of a radiotracer into the interstitial space in parallel with specific uptake. To the best of our knowledge, the characterization of specific versus passive components has not been thoroughly documented to date. According to this study, accumulation of the inactivated tracer in the area at risk peaked at ~ 30 min after injection and accounted for as much as 1 %ID/g, followed by a gradual washout. The data can be interpreted as extravasation of the tracer through compromised vascular structures and the diffusive distribution in interstitial space. During the initial period after injection, a high blood-pool concentration of the tracer favors infiltration into the area at risk. But with blood clearance, the shifting intravascular concentration drives the equilibrium toward a reversal and redistribution process as seen from the washout pattern. The timing and the degree of nonspecific uptake here are consistent with existing literature on ischemia- or reperfusion-induced vascular permeability changes measured using radiolabeled macromolecules and high-molecular-weight MR contrast agents (27,28). Although the binding of ^{99m}Tc -C2A-GST-NHS with unknown targets in the area at risk could not be completely ruled out, such interactions, if any, are likely to be relatively weak and transient as the tracer is washed out with declining blood-pool activity. On the other hand, the active molecular probe, ^{99m}Tc -C2A-GST, appears to

be sequestered in the area at risk. This uptake of ^{99m}Tc -C2A-GST is likely to consist of both specific and nonspecific components. The fact that the uptake level plateaued after 30 min may be a reflection of 2 dynamic components between a continuous accumulation due to specific binding and the vascular permeability-dependent diffusion equilibrium. The uptake of ^{99m}Tc -C2A-GST positively correlates with ischemia or reperfusion challenge that results in infarction and elevation of apoptotic index in the area at risk, whereas short stimulation with 5 min of ischemia followed by reperfusion causes no significant uptake of ^{99m}Tc -C2A-GST in the area at risk.

The in vivo imaging results were consistent with ex vivo uptake studies and demonstrated the feasibility of noninvasive imaging of acute infarction in small-animal models. When calibrated against the marker, which represents 0.5 %ID, region-of-interest analysis indicates that the lesion uptake at the heart correlates with 0.7 to 1 %ID. In healthy rats, ^{99m}Tc -C2A-GST clears from the blood pool in a well-defined profile. Meanwhile, the inactivated ^{99m}Tc -C2A-GST-NHS did not produce a target-to-background ratio that allows recognition of the infarct from the planar images.

CONCLUSION

With the synthesis and characterization of ^{99m}Tc -C2A-GST we describe the dynamic uptake of a PtdS-binding molecular probe in the area at risk. The data indicate that both specific binding and passive leakage due to vascular hyperpermeability contribute to the accumulation of the radiotracer at the area at risk. However, the latter component alone is insufficient to achieve detectable target-to-background ratios with in vivo planar imaging. On the basis of this study, C2A and its derivatives hold promise in becoming suitable radiopharmaceuticals for the noninvasive imaging of apoptosis and necrosis.

ACKNOWLEDGMENTS

The authors are grateful to Frank G. Steffel for his administrative support and David Peck for technical assistance. This work was supported in part by the American Heart Association (grant 0435147N).

REFERENCES

1. Kerr JF, Wyllie AH, Currie AR. Apoptosis: a basic biological phenomenon with wide-ranging implications in tissue kinetics. *Br J Cancer*. 1972;26:239-257.
2. Kerr JF. History of the events leading to the formulation of the apoptosis concept. *Toxicology*. 2002;181-182:471-474.
3. Selivanova G. p53: fighting cancer. *Curr Cancer Drug Targets*. 2004;4:385-402.
4. Huang P, Heimbrook DC. Oncogene products as therapeutic targets for cancer. *Curr Opin Oncol*. 1997;9:94-100.
5. Gourley M, Williamson JS. Angiogenesis: new targets for the development of anticancer chemotherapies. *Curr Pharm Des*. 2000;6:417-439.
6. Song Z, Steller H. Death by design: mechanism and control of apoptosis. *Trends Cell Biol*. 1999;9:M49-M52.
7. Wyllie AH. Apoptosis: an overview. *Br Med Bull*. 1997;53:451-465.
8. Grutter MG. Caspases: key players in programmed cell death. *Curr Opin Struct Biol*. 2000;10:649-655.
9. Green DR. Apoptotic pathways: the roads to ruin. *Cell*. 1998;94:695-698.

10. Thornberry NA, Lazebnik Y. Caspases: enemies within. *Science*. 1998;281:1312–1316.
11. Cohen GM. Caspases: the executioners of apoptosis. *Biochem J*. 1997;326:1–16.
12. Kostin S, Pool L, Elsasser A, et al. Myocytes die by multiple mechanisms in failing human hearts. *Circ Res*. 2003;92:715–724.
13. Freude B, Masters TN, Kostin S, et al. Cardiomyocyte apoptosis in acute and chronic conditions. *Basic Res Cardiol*. 1998;93:85–89.
14. Khaw BA. The current role of infarct avid imaging. *Semin Nucl Med*. 1999;29:259–270.
15. Williamson P, Schlegel RA. Transbilayer phospholipid movement and the clearance of apoptotic cells. *Biochim Biophys Acta*. 2002;1585:53–63.
16. Davletov BA, Sudhof TC. A single C2 domain from synaptotagmin I is sufficient for high affinity Ca^{2+} /phospholipid binding. *J Biol Chem*. 1993;268:26386–26390.
17. Zhao M, Beaugard DA, Loizou L, et al. Non-invasive detection of apoptosis using magnetic resonance imaging and a targeted contrast agent. *Nat Med*. 2001;7:1241–1244.
18. Jung HI, Kettunen MI, Davletov B, et al. Detection of apoptosis using the C2A domain of synaptotagmin I. *Bioconjug Chem*. 2004;15:983–987.
19. Blankenberg FG, Katsikis PD, Tait JF, et al. In vivo detection and imaging of phosphatidylserine expression during programmed cell death. *Proc Natl Acad Sci U S A*. 1998;95:6349–6354.
20. Ohtsuki K, Akashi K, Aoka Y, et al. Technetium-99m HYNIC-annexin V: a potential radiopharmaceutical for the in-vivo detection of apoptosis. *Eur J Nucl Med*. 1999;26:1251–1258.
21. Petrovsky A, Schellenberger E, Josephson L, et al. Near-infrared fluorescent imaging of tumor apoptosis. *Cancer Res*. 2003;63:1936–1942.
22. Lahorte CMM, VanderHeyden JL, Steinmetz N, et al. Apoptosis-detecting radioligands: current state of the art and future perspectives. *Eur J Nucl Med*. 2004;31:887–919.
23. Tait JF, Smith C, Blankenberg FG. Structural requirements for in vivo detection of cell death with $^{99\text{m}}\text{Tc}$ -annexin V. *J Nucl Med*. 2005;46:807–815.
24. Tait JF, Brown DS, Gibson DF, et al. Development and characterization of annexin V mutants with endogenous chelation sites for $^{99\text{m}}\text{Tc}$. *Bioconjug Chem*. 2000;11:918–925.
25. Hofstra L, Liem IH, Dumont EA, et al. Visualisation of cell death in vivo in patients with acute myocardial infarction. *Lancet*. 2000;356:209–212.
26. Thimister PW, Hofstra L, Liem IH, et al. In vivo detection of cell death in the area at risk in acute myocardial infarction. *J Nucl Med*. 2003;44:391–396.
27. Saeed M, van Dijke CF, Mann JS, et al. Histologic confirmation of microvascular hyperpermeability to macromolecular MR contrast medium in reperfused myocardial infarction. *J Magn Reson Imaging*. 1998;8:561–567.
28. Schwitter J, Saeed M, Wendland MF, et al. Influence of severity of myocardial injury on distribution of macromolecules: extravascular versus intravascular gadolinium-based magnetic resonance contrast agents. *J Am Coll Cardiol*. 1997;30:1086–1094.
29. Tesic M, Sheldon KM, Ballinger JR, et al. Labeling small quantities of monoclonal antibody and their F(ab')_2 fragments with technetium-99m. *Nucl Med Biol*. 1995;22:451–457.
30. Boyne AF, Ellman GL. A methodology for analysis of tissue sulfhydryl components. *Anal Biochem*. 1972;46:639–653.
31. Taki J, Higuchi T, Kawashima A, et al. Detection of cardiomyocyte death in a rat model of ischemia and reperfusion using $^{99\text{m}}\text{Tc}$ -labeled annexin V. *J Nucl Med*. 2004;45:1536–1541.
32. Sopkova J, Renouard M, Lewit-Bentley A. The crystal structure of a new high-calcium form of annexin V. *J Mol Biol*. 1993;234:816–825.
33. Huber R, Romisch J, Paques EP. The crystal and molecular structure of human annexin V, an anticoagulant protein that binds to calcium and membranes. *EMBO J*. 1990;9:3867–3874.
34. Huber R, Schneider M, Mayr I, et al. The calcium binding sites in human annexin V by crystal structure analysis at 2.0 Å resolution: implications for membrane binding and calcium channel activity. *FEBS Lett*. 1990;275:15–21.
35. Sutton RB, Davletov BA, Berghuis AM, et al. Structure of the first C2 domain of synaptotagmin I: a novel Ca^{2+} /phospholipid-binding fold. *Cell*. 1995;80:929–938.